Large and inverted spin signals in nonlocal spin valves

Han Zou, S. T. Chui, X. J. Wang, and Yi Ji

Phys. Rev. B **83**, 094402 — Published 3 March 2011

DOI: 10.1103/PhysRevB.83.094402

Large and inverted spin signals in nonlocal spin valves

Han Zou, S. T. Chui, X. J. Wang, and Yi Ji*

Department of Physics and Astronomy, University of Delaware, Newark, Delaware 19716

Abstract

A nonlocal spin valve (NLSV) is a nanoscale planar heterostructure, consisting of a spin injector, a spin detector, and a nonmagnetic channel. A pure spin current can be induced in the nonmagnetic channel by electrical spin injection. We report large but inverted spin signals in a set of NLSV structures. The interface between the ferromagnetic spin detector and the nonmagnetic channel is found to be a break-junction formed by electrostatic discharge. A large (> 80%) but negative tunneling spin polarization across the break-junction is inferred. The large magnitude is due to a strong coupling between the charges and spins at the low-conductance break-junction. The inverted sign results from the specific interfacial atomic structures and bonding states, which influences the spin-dependent tunneling matrices.

* corresponding author; yji@physics.udel.edu

Spin-based electronics[1, 2] (spintronics) has made profound impact on information technology by providing high density data storage devices and nonvolatile memories. The grand challenge for spintronics is to extend the Moore's law for nanoelectronics. Nonlocal spin valve (NLSV) structure[3] have been explored using both metallic[4-10] and semiconductor materials[11-14] due to its potential application for spintronics. The planar layout of the structure allows for complex spintronic devices[15] with multiple circuit elements such as input, output, and gate terminals.

A typical NLSV structure is shown in Fig. 1 (a). The injection of spins is accomplished by driving a charge current from the ferromagnetic (F) spin injector F_1 into the nonmagnetic channel (N), as shown in Fig. 1(b). A nonlocal voltage between the ferromagnetic spin detector F_2 and N is detected, converted to a spin signal, and related to the spin accumulation. The increase of the spin diffusion lengths λ_s of the N channel and the spin polarizations of the interfaces, P_1 for F_1/N and P_2 for F_2/N, is essential for enhancing the spin signals. We have observed a large (> 80%) but negative spin detection polarization (P_2) in NLSV structures with a break-junction at the F_2/N interface, in contrast to the positive and modest spin polarization (10 – 20%) for conventional F_2/N junctions. This indicates that a F/N break-junction can be used as a sensitive detector for spin accumulation.

Our NLSV devices are fabricated by electron-beam lithography followed by a shadow evaporation technique.[8, 16] A nanoscale suspended shadow mask is formed by e-beam lithography on two layers of resists with different sensitivities. Magnetic materials (F), aluminum oxide (AlO_x), and nonmagnetic materials (N) are deposited from different

angles through the shadow mask subsequently. The NLSV planar heterostructure is formed without breaking vacuum. The final structure is obtained after a lift-off process in which the resists are removed. A scanning electron microscope (SEM) picture of the finished NLSV structure is shown in Fig. 1 (a). The N channel is made of Cu and the F_1 (spin injector) and F_2 (spin detector) electrodes are made of Co or Py (NiFe alloy). There is a 2 nm AlO_x layer at the F_1/Cu and F_2/Cu interfaces. The oxide layer at F/N interface has been shown to increase the values of P_1 and P_2 for NLSV structures.[7, 17-19] The width of the Cu channel is 100 – 120 nm and widths of F_1 and F_2 electrodes are typically 60 – 80 nm. The center-to-center distance between F_1 and F_2 varies between 200 and 500 nm.

A cartoon illustration of the structure and the measurement configuration is shown in Fig. 1 (b). The F_1 and F_2 electrodes extend underneath the Cu channel, which is 80 - 100 nm thick. The F_1 electrode is a 10 -15 nm magnetic layer. The F_2 electrode is either an 8 nm uniform magnetic layer or a 3 nm magnetic layer with a 5 nm Cu under-layer. The purpose of the Cu under-layer is to ensure electrical continuity of the F_2 electrode. The inverted large spin signals are observed in both types. An injection current is directed from F_1 into the Cu, resulting in a spin accumulation in the Cu and a pure spin current flowing toward F_2. The nonlocal voltage V_s between F_2 and the Cu channel is high when the spin polarization of F_2 is parallel with the spin accumulation in Cu, and low when antiparallel. The measurements of V_s are carried out using a.c. lock-in technique at low frequency (< 1 kHz) The voltage difference ΔV_s between two states normalized by the injection current I is known as the spin signal ΔR_s.

The spin polarization of the current through the F/N interfaces is defined as $P = \frac{I_\uparrow - I_\downarrow}{I_\uparrow + I_\downarrow}$, where $I_\uparrow$ and $I_\downarrow$ are the spin-up and spin-down components of the current,

respectively. Spin-up direction is the majority spin (magnetization) direction of the F metal. Measurements of tunneling spin polarizations from ferromagnets have primarily indicated positive signs.[20] But the tunneling polarization is sensitive to the detailed atomic structures near the interfaces[21-23] and a negative polarization can arise from certain types of tunnel barriers.[24-27]

The measurement for an ordinary Co-Cu NLSV is shown in Fig. 2. The normalized nonlocal voltage $R_s = V_s/I$ is plotted versus magnetic field H at 4.2 K and 295 K in Fig. 2 (a) and (b), respectively. The F_1 and F_2 have different switching fields due to different thicknesses, and parallel or antiparallel magnetizations can be reached by sweeping the magnetic field. The ΔR_s = 6 mΩ at both 295 K and 4.2 K. The high value of R_s corresponds to the parallel magnetizations of F_1 and F_2 and the low value of R_s to the antiparallel state. This is consistently observed in previous metallic NLSV measurements, because the spin polarizations of the F_1 and F_2 have the same signs. If the spin polarizations have opposite signs, an inverted spin signal would be obtained with a low R_s value for the parallel state and high R_s value for the antiparallel state.

The spin signal is described[28] by

$$\Delta R_s = \frac{P_1 P_2 \rho \lambda_s}{A} e^{-\frac{L}{\lambda_s}}, \qquad (1)$$

where P_1 and P_2 are the spin polarization of the F_1/Cu and F_2/Cu interfaces, ρ is the resistivity of the Cu, λ_s is the spin diffusion length of the Cu, A is the cross sectional area of the Cu channel, and L is the distance between F_1 and F_2. For an ordinary NLSV, L should be the center-to-center separation. The Cu resistivity ρ = 1.1 μΩ·cm at 4.2 K and 2.8 μΩ·cm at 295K. For this device, $A = 120 \times 100$ nm^2 and L = 200 nm. An accurate

determination of P_1, P_2, and λ_s requires measuring a series of devices with varying L. Our measurements on many NLSV structures yield 10 - 20 % polarizations (P_1 or P_2) for Co/AlO_x/Cu interfaces, depending on the Co and AlO_x thicknesses. The λ_s is 400 - 800 nm at 4.2 K and 250 - 400 nm at 295 K. We estimate $P_1 = P_2 = 14\%$ and $\lambda_s = 500$ nm for the ΔR_s of 6 mΩ at 4.2 K. At 295 K the λ_s decreases to 275 nm but ρ increases to 2.8 μΩ·cm, resulting in the same ΔR_s of 6 mΩ. We assume that the polarizations are the same for 4.2 K and 295 K. This assumption is supported by our detailed measurements on **Co** based NLSV structures.[29, 30] In the literature[31, 32] as well as in our measurements, spin signals in the different **Py** based NLSV structures decrease by a factor of 2 or more as temperature increases from 4.2 K to room temperature due to a decrease of the spin polarizations.

In this paper, we focus on a set of NLSV devices which are apparently fabricated using the same methods and materials but behave quite differently. The measurement of such a Co-Cu device at 4.2 K is shown in Fig. 3(a). A striking feature is that spin signal is inverted: the R_s is low for the parallel state and high for the antiparallel state of F_1 and F_2, opposite to that previously discussed. In addition, the ΔR_s of 15 mΩ is higher than the 6 mΩ in Fig. 2. While this device is immersed in the cryostat, we measured the resistances at F_1/Cu and F_2/Cu interfaces in-situ. The resistance of F_1/Cu is 200 Ω, similar to that of ordinary NLSV with Co/AlO_x/Cu interfaces.[17] The resistance of F_2/Cu, however, is extraordinarily large (> 100 MΩ). Subsequently we measured the R_s versus H curve (shown in Fig. 3(b)) again at 4.2 K and found that the inverted ΔR_s is increased by a factor of 6 to 90 mΩ. We note that the R_s versus H curves in Fig 3 are **well reproducible** during continuous field sweeps. The inverted sign of the ΔR_s observed here should not be

confused with the sign reversal associated with a reversal of the direction of the d.c. injection current.[33] In addition, the electrical wiring configurations have been carefully confirmed to be consistent with Fig. 1(b), and the possibility of an inverted sign due to incorrect wirings can be ruled out. Our measurements use a.c. lock-in technique and the in-phase component of the signal is measured.

The experiments indicate that a high resistance but delicate interface with high spin polarization, *i.e.* a break-junction tunnel barrier, is formed between the Py (F_2) electrode and the Cu channel. The formation of the break junction is due to electrostatic discharge and the thinner F_2 electrode is more susceptible than F_1. The initial breaking likely occurs when the device in the cryostat is connected to the measurement equipments, resulting in the 15 mΩ inverted signal. The interface resistance measurements require rearrangement of the wiring configurations, which induces additional electrostatic discharge. The break-junction is therefore modified through electromigration and a larger spin signal of 90 mΩ arises. We have inspected all devices with inverted spin signals in SEM after the measurements and no apparent gap is seen between F_2 and Cu. The break-junction should be no more than a few nanometers, smaller than the resolution of SEM.

The electrostatic breakdown should occur where the Py detector (F_2) connects with the Cu channel. This is the weakest spot in the entire device where electrostatic breakdown often occurs. The break-junction is actually a vacuum gap between the F_2 and the Cu instead of a pinhole at the F_2/AlO_x /Cu interface. Once the break-junction is formed, electrons tunnel laterally from F_2 into Cu through the vacuum gap instead of vertically through the F_2/AlO_x/Cu interface.

A large P_2 for the F_2/Cu interface is necessary to account for a ΔR_s of 90 mΩ. In the following, we estimate the lower limit of P_2 by maximizing the contributions to ΔR_s from other factors. For this device $A = 130 \times 100$ nm^2 and the center-to-center separation is 190 nm. However, the break-junction is not necessarily located at the center of the F_2 electrode. The situation that maximizes ΔR_s is: the break-junction is located on the F_2 edge that is closer to F_1, and therefore $L = 155$ nm. We assume $P_1 = 20\%$ and $\lambda_s = 800$ nm, the highest values observed in ordinary Co-Cu NLSV. Then an 80% polarization is inferred and it is the lower bound for the P_2 through the F_2/Cu break-junction, i.e. $P_2 > 80\%$. For the ΔR_s of 15 mΩ in Fig 3 (a), we conclude $P_2 > 13\%$ using a similar approach.

The inverted spin signal has been observed in five NLSV structures including both Co-Cu and Py-Cu types. A plot of R_s versus H with an inverted 58 mΩ at 4.2 K is shown in Fig 3 (c) for a Py-Cu structure with $A = 70 \times 100$ nm^2 and a 480 nm center-to-center separation. A similar estimate indicates that $P_2 > 40\%$.

Recently spin-related thermoelectric effects have been reported.[34, 35] However, the large spin signals observed in this work can not be explained by thermal effects. The thermal power by Joule heating is given by the square of the voltage across the junction divided by the junction resistance. This is actually reduced in the present case by the large resistance of the break-junction. Furthermore, there is no applied charge voltage across the F_2/N interface in the nonlocal device, unlike conventional spin valves or tunnel junctions. In addition, the spin signals due to thermal effects are small and appear on the second harmonic of the lock-in measurements.[35]

In the following, we present a model that explains why a break junction causes a large effective spin polarization. In spin polarized transport in ferromagnets the spin and

charge are coupled.[36, 37] This originates from the fact that the two spin species have different conductivities (σ_{+1} for spin-up and σ_{-1} for spin-down) and diffusion constants (D_{+1} for spin-up and D_{-1} for spin-down) in a ferromagnet. The diffusion of for each specie can be described by $\mathbf{J_s} = -\sigma_s \nabla V - D_s \nabla \delta n_s$, where $s = \pm 1$ (+1 for spin-up and -1 for spin-down), δn_s is the deviation of population density from the equilibrium for spin s, and $\mathbf{J_s}$ is the current density for spin s. We have used units so that the Bohr magneton and the electric charge is 1. The electric potential V includes the potential due to the external electric field and the local electric (screening) potential due to charge accumulation. The charge accumulation is defined by $\delta n = \delta n_{+1} + \delta n_{-1}$, and the spin accumulation is defined by $\delta M = (\delta n_{+1} - \delta n_{-1})$. We assume that the local equilibrium magnetization $\mathbf{M_0}$ lies along the z direction and that it is a longitudinal spin accumulation which also lies along the z direction. The charge current is defined by $\mathbf{J_e} = \mathbf{J_+} + \mathbf{J_-}$, and the spin current is defined by $\mathbf{J_M} = \mathbf{J_+} - \mathbf{J_-}$.

It follows from the above that both $\mathbf{J_e}$ and $\mathbf{J_M}$ are related to the spin accumulation δM and the charge accumulation δn:

$$\mathbf{J}_e = -\sigma \nabla V - D \nabla(\delta n) - D' \nabla(\delta M) \qquad (2)$$

$$\mathbf{J}_M = -\sigma' \nabla V - D \nabla(\delta M) - D' \nabla(\delta n) \qquad (3)$$

where $\sigma = (\sigma_{+1} + \sigma_{-1})/2$, $\sigma' = (\sigma_{+1} - \sigma_{-1})/2$, $D = (D_{+1} + D_{-1})/2$ and $D' = (D_{+1} - D_{-1})/2$. In addition, the charge density satisfies the condition of global charge current conservation. In the steady state the divergence of charge current vanishes:

$$\nabla \cdot \mathbf{J_e} = \frac{\partial \delta n}{\partial t} = 0 \qquad (4).$$

The magnetization satisfies the modified Landau-Gilbert equation with a source term proportional to the divergence of the magnetization. In the steady state with a longitudinal spin accumulation, we have

$$\nabla \cdot \mathbf{J}_{\mathbf{M}} = -\frac{\delta M}{\tau} \qquad (5),$$

where τ is the spin relaxation time. We solve Eq. (2-5) for the charge accumulation δn and the spin accumulation δM.

In Eq. (2) and (3), the δn and the δM are coupled through terms involving D' and σ'. In the special case of a nonmagnetic metal (N) where $D' = 0$ and $\sigma' = 0$, the spins and the charges are decoupled. Eq. (2) and (4) describes the charge accumulation alone and gives rise to the conclusion that the δn decays on the scale of the screening length which is defined by $\lambda_c = \sqrt{\frac{D}{4\pi\sigma}}$. Eq. (3) and (5) describes the spin accumulation alone and give rise to the conclusion that the δM decays on the scale of the spin diffusion length which is defined by $\lambda_s = \sqrt{D\tau}$.

For F metals, the D' and σ' are non-vanishing. The δn and δM are coupled in Eq. (2) and (3), and therefore the solutions of δn or δM to Eq. (2-5) splits into two terms. One term, δM_c (or δn_c), decays on the scale of a renormalized screening length λ_c', which is close to value of λ_c, but more precisely related to λ_c, D and D'. The other term, δM_s (or δn_s), decays on the scale of a renormalized spin diffusion length λ_s', which is close to the value of λ_s, but more precisely related to λ_s, D and D'. In F metals the value of λ_c is of the order of 0.1 nm and the value of λ_s is of the order of 10 nm. For a NLSV with a F_2/N

break-junction, the δM_c term dominates close to the F_2 side of break-junction interface and it is responsible for the large inverted spin signal. This will be discussed in more detail later.

The boundary conditions are that the $\mathbf{J_e}$ and $\mathbf{J_M}$ are continuous across the F/N interfaces (F_1/N and N/F_2). When the $\mathbf{J_M}$ values (or $\mathbf{J_e}$) in two metals across the interface are matched, the bulk and the interfacial spin-dependent transport parameters appear in the solution of δM. These parameters can be organized into an effective interfacial conductance ($c^{F1/N}$ or $c^{F2/N}$) for each F/N interface and a metallic conductance c_m of each bulk metallic component. As an example, the $c^{F2/N}$ is defined as

$$c^{F2/N} = \sum_{s=\pm 1} | T_s^{F2/N} |^2 \, [1 + s\gamma(1 + \lambda_{cF} / \lambda_{cN})] \qquad (6).$$

The parameter $T_{\pm 1}^{F2/N}$ is proportional to the tunneling matrix element for the F_2/N interface for spin-up (+1) and spin-down (-1). $\gamma = 1 + D/D'$ is a measure of the spin asymmetry of the diffusion constants of the ferromagnet. For a break-junction F_2/N interface, $c^{F2N} << c_m$.

The solutions of δM across a F_2/N interface with low conductance are shown in Fig. 4. There is a single term of δM (δM_s only) inside N but two separate terms (δM_c and δM_s) inside F_2, as explained earlier. The distance 0 is at the F_2/N interface, a negative distance is inside N, and a positive distance is inside F_2. The magnitude of the magnetization current density $\mathbf{J_M}$ arriving at the F_2/N is determined by the conductance of the F_1/N interface. This $\mathbf{J_M}$ in a NLSV with a break-junction at F_2/N should be the same as that in an ordinary NLSV, since the F_1/N interfaces are the same in both structures. The

magnitude of δM_c at distance of 0^+ (inside F_2) is inversely proportional to the effective conductance $c^{F2/N}$ of the F_2/N interfaces. The magnitude of δM_s at distance of 0^+ is inversely proportional to the metallic conductance c_m of F_2. While c_m does not vary substantially for F metals, $c^{F2/N}$ may vary by orders of magnitudes depending on the nature of the F_2/N interface. For a highly conductive N/F_2 interface, δM_c is small and δM_s is the major contribution to the total spin accumulation δM at distance of 0^+. This is the case for ordinary NLSV structures, where both N/F interfaces are fairly conductive, and the spin signals ΔR_s primarily come from δM_s. For highly resistive N/F_2 interface, such as a break-junction, a much higher δM_c arises and dominates over δM_s at distance of 0^+. The measured spin signals ΔR_s are primarily attributed to δM_c and are much higher than those in ordinary NLSV. This is the case shown in Fig. 4.

The coupling between spins and charges can be viewed intuitively as a charge dipole layer in addition to a magnetization dipole layer across the N/F_2 interface. A low-conductance N/F_2 interface gives rise to a high capacitance and therefore a large charge dipole, which implies a strong charge-spin coupling and therefore large δM_c and ΔR_s are induced. Since δM_c decays rapidly over distance away from the interface, it can be interpreted as a large effective interfacial spin polarization P_2 at the break-junction N/F_2 interface.

A sign change occurs for δM_c and ΔR_s, if the $c^{F2/N}$, defined in Eq. (6), changes its sign. A sign change of $c^{F2/N}$ can be induced when the magnitudes of tunneling matrices changes from $T_{-1}^{F2/N} < T_{+1}^{F2/N}$ (the tunneling matrix for minority spins is lower than that of the majority spins) to $T_{-1}^{F2/N} > T_{+1}^{F2/N}$ (the tunneling matrix for minority spins is higher

than that of the majority spins). A negative $c^{F2/N}$ and negative tunneling spin polarization can arise from the latter with a reasonable choice of parameters in Eq. (6). The density of states near a break-junction can be substantially different from that of the bulk due to the low coordination number of atoms.[23] A negative tunneling spin polarization from ordinary transition metals is rare but has been observed for break-junctions[27] and $SrTiO_3$ barriers.[24-26] Calculations[21, 22] have shown that interfacial bonding with oxygen[21] can change the sign of spin polarization of transition metals. In our device, there is the coexistence of Co (or Py), Cu, Al, and O atoms near the break-junctions and complex bonding states may arise. The detailed mechanism for the inverted sign is subject to further investigations.

In conclusion, we have observed large inverted spin signals in nanoscale nonlocal spin valves. A large (> 80%) but negative spin detection polarization is inferred for the break-junction interface between the magnetic spin detector and the Cu channel. The large magnitude is attributed to a strong coupling between spins and charges, which induces a large spin accumulation at the interface that decays on the scale of charge screening length. The negative sign is due to the interfacial electronic and atomic structures near the break-junctions.

We acknowledge use of University of Maryland NanoCenter facilities. This work was supported by US DOE grant No. DE-FG02-07ER46374.

References

[1] S. A. Wolf, D. D. Awschalom, R. A. Buhrman, et al., Science **294**, 5546 (2001).

[2] I. Zutic, J. Fabian, and S. Das Sarma, Reviews of Modern Physics **76**, 323 (2004).

[3] M. Johnson and R. H. Silsbee, Physical Review Letters **55**, 1790 (1985).

[4] F. J. Jedema, A. T. Filip, and B. J. van Wees, Nature **410**, 345 (2001).

[5] F. J. Jedema, H. B. Heersche, A. T. Filip, et al., Nature **416**, 713 (2002).

[6] T. Kimura, J. Hamrle, Y. Otani, et al., Applied Physics Letters **85**, 3501 (2004).

[7] S. O. Valenzuela and M. Tinkham, Applied Physics Letters **85**, 5914 (2004).

[8] Y. Ji, A. Hoffmann, J. E. Pearson, et al., Applied Physics Letters **88**, 052509 (2006).

[9] S. Garzon, I. Zutic, and R. A. Webb, Physical Review Letters **94**, 176601 (2005).

[10] R. Godfrey and M. Johnson, Physical Review Letters **96**, 136601 (2006).

[11] O. M. J. van't Erve, A. T. Hanbicki, M. Holub, et al., Applied Physics Letters **91**, 212109 (2007).

[12] X. H. Lou, C. Adelmann, S. A. Crooker, et al., Nature Physics **3**, 197 (2007).

[13] D. Saha, M. Holub, and P. Bhattacharya, Applied Physics Letters **91**, 072513 (2007).

[14] H. C. Koo, J. H. Kwon, J. Eom, et al., Science **325**, 1515 (2009).

[15] T. Kimura and M. Hara, Applied Physics Letters **97**, 182501 (2010).

[16] Y. Ji, A. Hoffmann, J. S. Jiang, et al., Journal of Physics D-Applied Physics **40**, 1280 (2007).

[17] X. J. Wang, H. Zou, L. E. Ocola, et al., Applied Physics Letters **95**, 022519 (2009).

[18] Y. Fukuma, L. Wang, H. Idzuchi, et al., Applied Physics Letters **97**, 012507 (2010).

[19] A. Vogel, J. Wulfhorst, and G. Meier, Applied Physics Letters **94**, 122510 (2009).

[20] R. Meservey and P. M. Tedrow, Physics Reports-Review Section Of Physics Letters **238**, 173 (1994).

[21] K. D. Belashchenko, E. Y. Tsymbal, M. van Schilfgaarde, et al., Physical Review B **69** (2004).

[22] E. Y. Tsymbal and K. D. Belashchenko, Journal Of Applied Physics **97** (2005).

[23] D. Jacob, J. Fernandez-Rossier, and J. J. Palacios, Physical Review B **71**, 220403 (2005).

[24] J. M. De Teresa, A. Barthelemy, A. Fert, et al., Physical Review Letters **82**, 4288 (1999).

[25] J. M. De Teresa, A. Barthelemy, A. Fert, et al., Science **286**, 507 (1999).

[26] D. C. Worledge and T. H. Geballe, Physical Review Letters **85**, 5182 (2000).

[27] K. I. Bolotin, F. Kuemmeth, A. N. Pasupathy, et al., Nano Letters **6**, 123 (2006).

[28] S. Takahashi and S. Maekawa, Physical Review B **67**, 052409 (2003).

[29] X. J. Wang, H. Zou, and Y. Ji, Physical Review B. **81**, 104409 (2010).

[30] X. J. Wang, H. Zou, and Y. Ji, Journal of Magnetism And Magnetic Materials **322**, 3572 (2010).

[31] G. Mihajlovic, J. E. Pearson, S. D. Bader, et al., Physical Review Letters **104**, 237202 (2010).

[32] T. Kimura, T. Sato, and Y. Otani, Physical Review Letters **100**, 066602 (2008).

[33] F. Casanova, A. Sharoni, M. Erekhinsky, et al., Physical Review B. **79**, 184415 (2009).

[34] K. Uchida, S. Takahashi, K. Harii, et al., Nature **455**, 778 (2008).

[35] A. Slachter, F. L. Bakker, J. P. Adam, et al., arXiv:1004.1566 (2010).

[36] S. T. Chui and Z. F. Lin, Physical Review B **77**, 094432 (2008).

[37] S. T. Chui, "Multiple magnetic tunnel junctions", US patent # 5757056 (1998).

Figure Captions

Figure 1. (a) Scanning electron microscope picture of a NLSV device; (b) A cartoon illustration of the NLSV structure with different colors representing different materials.

Figure 2. Plots of R_s versus H at 4.2 K (a) and 295 K (b) for an ordinary NLSV device. The blue arrows indicate the magnetization directions of F_1 and F_2.

Figure 3. Plots of R_s versus H showing inverted spin signals at 4.2 K (a) for a Co-Cu device; (b) for the same Co-Cu device after interface resistance measurements; (c) for a Py-Cu device.

Figure 4. The theoretical magnitude of spin accumulation $|\delta M|$ across the N/F_2 interface. On the N side, $|\delta M|$ decays on the scale of spin diffusion length λ_s of the nonmagnetic metal. On the F_2 side, $|\delta M_s|$ decays on the scale of λ_s of the ferromagnetic metal and $|\delta M_c|$ decays on the scale of charge screening length λ_c. For a low-conductance N/F_2 interface, the magnitude of $|\delta M_c|$ is much higher than that of $|\delta M_s|$ at distance of 0^+.

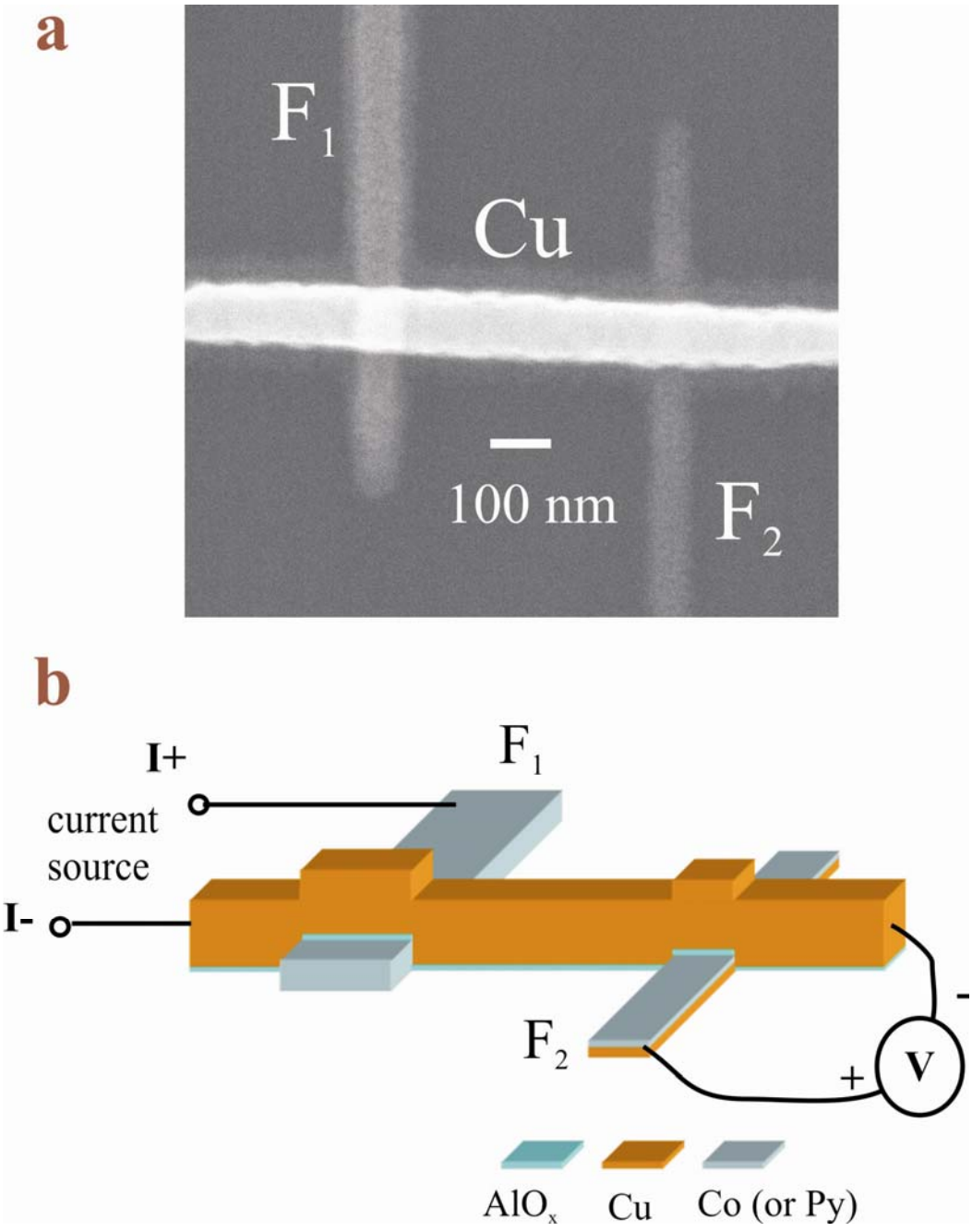

Figure 1

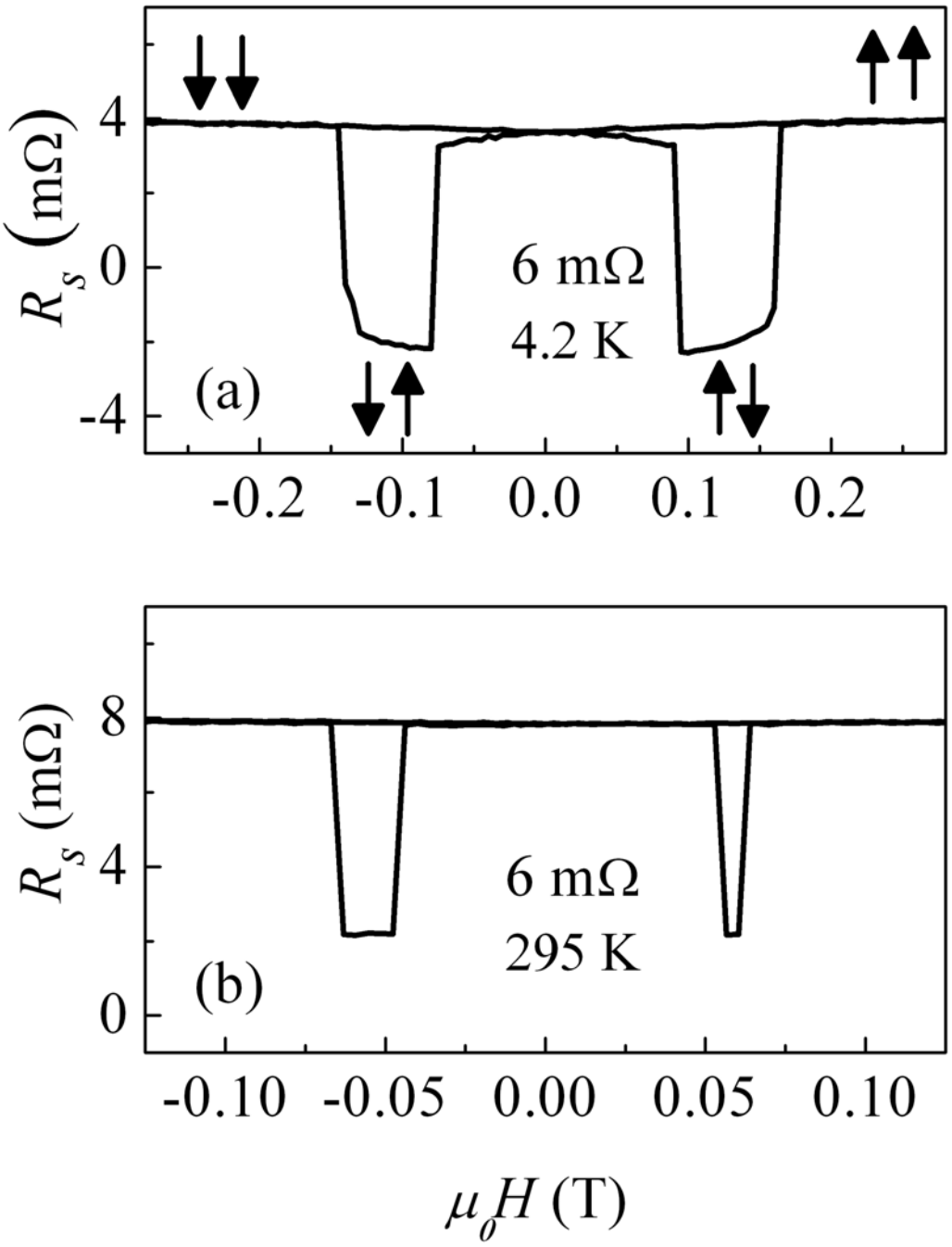
4
0
-4
R_s (mΩ)
6 mΩ
4.2 K
(a)
-0.2
-0.1
0.0
0.1
0.2
8
4
0
R_s (mΩ)
6 mΩ
295 K
(b)
-0.10
-0.05
0.00
0.05
0.10
$\mu_0 H$ (T)

Figure 2

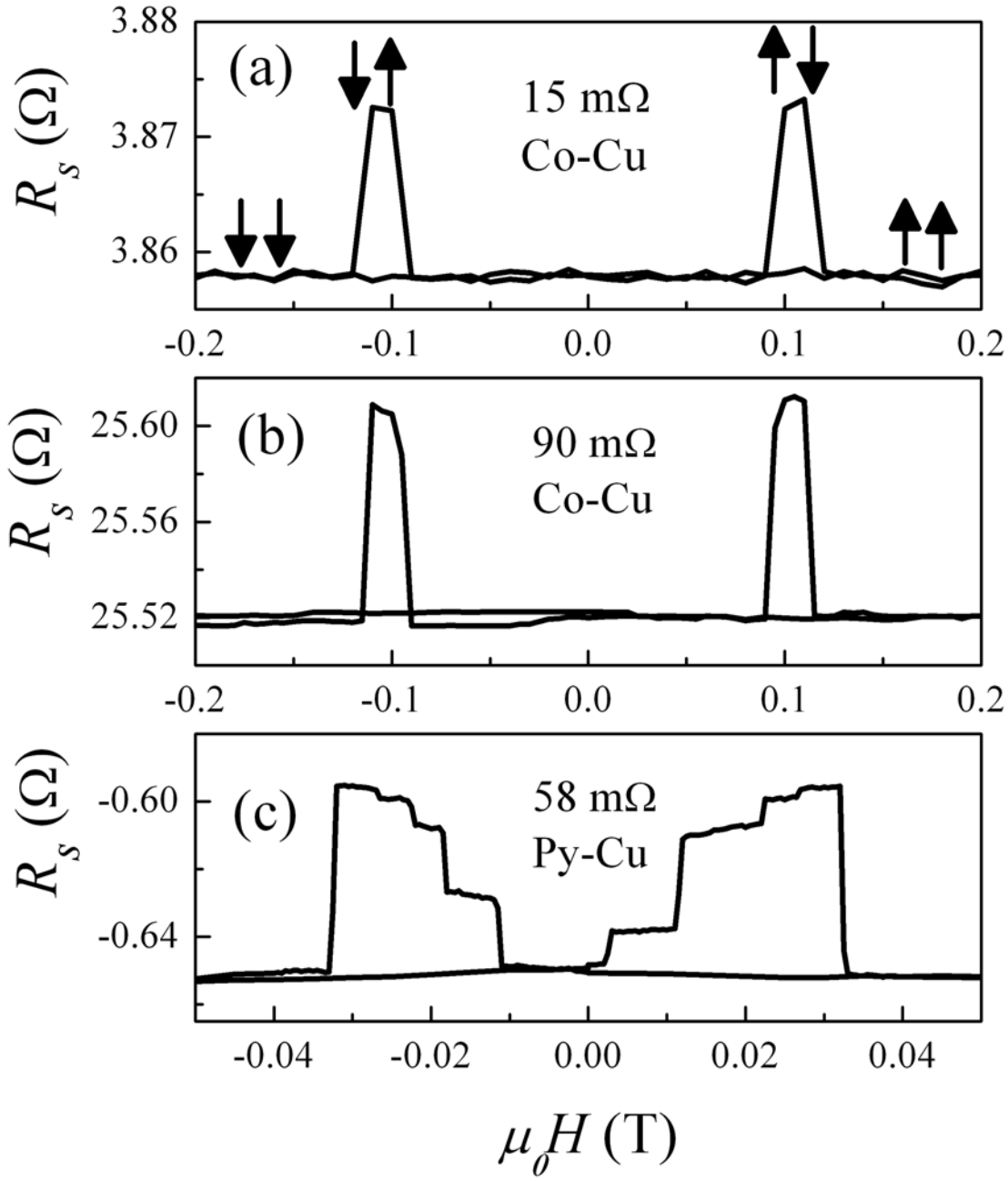
(a)
15 mΩ
Co-Cu
(b)
90 mΩ
Co-Cu
(c)
58 mΩ
Py-Cu
R_s (Ω)
3.88
3.87
3.86
25.60
25.56
25.52
-0.60
-0.64
-0.2
-0.1
0.0
0.1
0.2
-0.04
-0.02
0.00
0.02
0.04
$\mu_0 H$ (T)

Figure 3

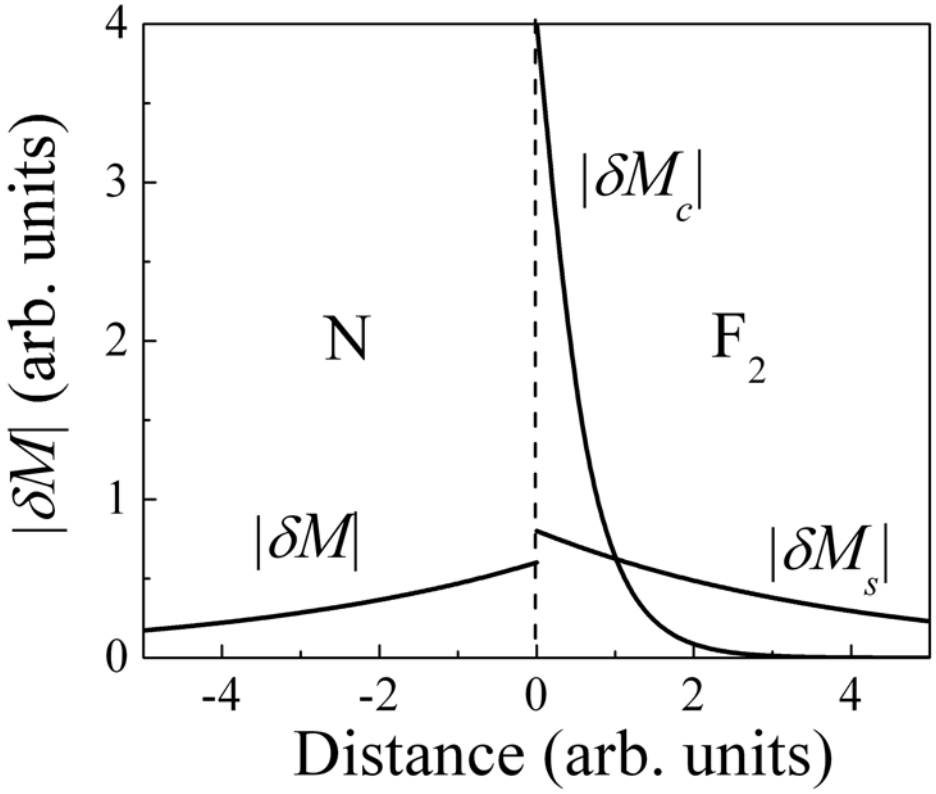

Figure 4